

Effect of dentin matrix components on the mineralization of human mesenchymal stromal cells

Petridis, Xenos; Beems, Bas Pieter; Tomson, Phillip; Scheven, Ben; Giepmans, Ben; Kuipers, Jeroen; van der Sluis, Luc; Harmsen, Martin C

DOI:

[10.1089/ten.TEA.2018.0192](https://doi.org/10.1089/ten.TEA.2018.0192)

License:

None: All rights reserved

Document Version

Peer reviewed version

Citation for published version (Harvard):

Petridis, X, Beems, BP, Tomson, P, Scheven, B, Giepmans, B, Kuipers, J, van der Sluis, L & Harmsen, MC 2018, 'Effect of dentin matrix components on the mineralization of human mesenchymal stromal cells', *Tissue Engineering Part A*. <https://doi.org/10.1089/ten.TEA.2018.0192>

[Link to publication on Research at Birmingham portal](#)

Publisher Rights Statement:

Checked for eligibility 03/12/2018

"Final publication is available from Mary Ann Liebert, Inc., publishers <http://dx.doi.org/10.1089/ten.TEA.2018.0192>

General rights

Unless a licence is specified above, all rights (including copyright and moral rights) in this document are retained by the authors and/or the copyright holders. The express permission of the copyright holder must be obtained for any use of this material other than for purposes permitted by law.

- Users may freely distribute the URL that is used to identify this publication.
- Users may download and/or print one copy of the publication from the University of Birmingham research portal for the purpose of private study or non-commercial research.
- User may use extracts from the document in line with the concept of 'fair dealing' under the Copyright, Designs and Patents Act 1988 (?)
- Users may not further distribute the material nor use it for the purposes of commercial gain.

Where a licence is displayed above, please note the terms and conditions of the licence govern your use of this document.

When citing, please reference the published version.

Take down policy

While the University of Birmingham exercises care and attention in making items available there are rare occasions when an item has been uploaded in error or has been deemed to be commercially or otherwise sensitive.

If you believe that this is the case for this document, please contact UBIRA@lists.bham.ac.uk providing details and we will remove access to the work immediately and investigate.

Effect of dentin matrix components on the mineralization of human mesenchymal stromal cells

Xenos Petridis^{1a*}, Bas P. Beems^{1b*}, Phillip L. Tomson^{2c}, Ben Scheven^{2d}, Ben N.G. Giepmans^{3e}, Jeroen Kuipers^{3e}, Luc W. M. van der Sluis^{1f}, Martin C. Harmsen^{4g}

¹University of Groningen, University Medical Center Groningen, Center for Dentistry and Oral Hygiene, Groningen, The Netherlands

²School of Dentistry, Institute of Clinical Sciences, College of Medical and Dental Sciences, University of Birmingham, Birmingham, UK

³University of Groningen, University Medical Center Groningen, Department of Cell Biology, Groningen, The Netherlands

⁴University of Groningen, University Medical Center Groningen, Department of Pathology and Medical Biology, Groningen, The Netherlands

** Both authors have contributed equally to this study and should be mentioned as first authors.*

^aCorresponding Author: Xenos Petridis, telephone: +31 629464747, e-mail: x.petridis@umcg.nl

^bBas Beems, telephone: +31 647302746, email: b.p.beems@umcg.nl

^cDr. Phillip Tomson, telephone: +44 1214665173, email: p.l.tomson@bham.ac.uk

^dDr. Ben Scheven, telephone: +44 1214665480, email: b.a.scheven@bham.ac.uk

^eDr. Ben Giepmans, telephone +31 503616133, email: b.n.g.giepmans@umcg.nl

^eDr. Jeroen Kuipers, telephone +31 612983675, email: j.kuipers05@umcg.nl

^fDr. Luc van der Sluis, telephone: +31 652773497, email: l.w.m.van.der.sluis@umcg.nl

^gProf. Dr. Martin Harmsen, telephone: +31 503614776, email: m.c.harmsen@umcg.nl

Abstract

In teeth with an injured pulp, dentin matrix orchestrates hard tissue repair through the release of dentin extracellular matrix components (dEMCs). dEMCs regulate the differentiation of resident mesenchymal stromal cells (MSCs), thereby affecting mineral deposition. Here, we show that low concentration solubilized dEMCs in osteogenic cultures of human umbilical cord mesenchymal stromal cells (UC-MSCs) and dental pulp stromal cells (DPSCs) enhanced mineral deposition, while adipose stromal cells (ASCs) were barely affected. Interestingly, UC-MSCs displayed significantly greater hydroxyapatite formation compared to DPSCs. UC-MSCs and DPSCs showed a dose-dependent viability and proliferation, whereas proliferation of ASCs remained unaffected. Qualitative analysis of the dEMCs-supplemented osteogenic cultures through scanning electron microscopy demonstrated differences in the architecture of the deposited mineralized structures. Large-sized mineral accretions upon a poorly organized collagen network was the prominent feature of UC-MSCs cultures, while mineral nodules interspersed throughout a collagen mesh were observed in the respective DPSCs cultures. The ability of dEMCs to induce mineralization varies between different human MSCs types in terms of total mineral formation and its architecture. Mineral formation by UC-MSCs exposed to low concentration dEMCs proved to be the most efficient and therefore could be considered as a promising combination for mineralized tissue engineering.

Keywords: dental pulp, dentin matrix, mesenchymal stromal cells, mineralization, tissue engineering, umbilical cord

Impact Statement

This research has been conducted with the aim to contribute to the development of treatment modalities for the reconstruction of lost/ damaged mineralized tissues. Currently, determining the most appropriate stromal cell population and signaling cues stand at the core of developing effective treatments. We provide new insights into the effect of innate inductive cues found in human dentin matrix components, on the osteogenic differentiation of various human stromal cell types. The effects of dEMCs on umbilical cord mesenchymal stromal cells has not been investigated before. The findings

of this study could underpin translational research based in the development of techniques for mineralized tissue engineering and will be of great interest for the readership of Tissue Engineering Part A.

Introduction

An effective approach to generate mineralized tissues requires mesenchymal stromal cells (MSCs) with osteogenic potential, suitable scaffolds and molecules that deliver differentiation-inductive signals^{1,2}. MSCs from bone marrow (BM-MSCs), adipose tissue (ASCs) and dental pulp (DPSCs) are often employed in mineralizing tissue engineering and regenerative strategies³. However, issues related to decreased cell number and osteogenic plasticity associated with ageing, as well as the invasive harvesting procedures to obtain them could limit their large-scale use^{4,5}. Besides the afore-mentioned adult MSCs, the mineralization potential of cells isolated from the umbilical cord stroma (UC-MSCs) has been documented both *in vitro* and *in vivo*^{6,7}. Indeed, their use might be advantageous due to their primitive state and the high cell yield obtained through non-invasive harvesting.

The dentin extracellular matrix has been shown to influence the reparative processes in the dentin hard tissue⁸. Physiologically, it is laid down by terminally differentiated cells, the odontoblasts, and its basic structural compound is collagen. Collagens form a cross-linked scaffold together with various non-collagenous proteins (NCPs) upon which minerals are deposited⁹. Among the NCPs, Small Integrin-Binding Ligand N-linked Glycoproteins (SIBLINGs), such as dentin sialoprotein (DSP), dentin phosphoprotein (DPP), bone sialoprotein (BSP), dentin matrix protein-1 (DMP-1), osteopontin, and matrix extracellular phosphoglycoprotein (MEPE), Small Leucine-Rich Proteoglycans (SLRPs) and osteocalcin are present in abundance, as well as a range of growth factors⁸. The latter include the transforming growth factor- β (TGF- β) superfamily, insulin-like growth factor 1 and 2 (IGF-1 and -2) and fibroblast growth factor-2 (FGF-2)⁸. Importantly, these signaling molecules are also released secondary to processes that cause dentin dissolution (e.g. dental caries) and contribute to providing the necessary cues required to mediate endogenous precursor stromal cells to lay down extracellular matrix leading to hard tissue repair at the site of injury⁸.

Due to the compositional similarities that mineralized tissues exhibit, dentin emerges as an 'easy-to-harvest' source of potent signaling molecules to promote mineralized tissue repair¹⁰. Effective use of dentin in mineralized tissue engineering requires precise

processing of the extracellular matrix in order to facilitate the extraction of its bioactive molecules. Solubilization is a crucial procedural step in extracting dentin matrix proteins. Employing EDTA as a demineralizing agent shows predictable and high extraction efficiencies for a variety of bioactive growth factors and NCPs that participate in mineralization, such as TGF- β 1, BMP-2, FGF-2, IGF-1, VEGF, PDGF, biglycan and decorin¹¹⁻¹⁸.

Demineralized dentin extracts containing dentin extracellular matrix components (dEMCs) induce the osteoblastic differentiation of human BM-MSCs¹⁶. The efficacy of dEMCs on augmenting DPSCs mineralization has also been demonstrated^{13,19}. Davies et al.²⁰ have shown that dEMCs can act in synergy with osteogenic-supplemented culture media and enhance mineralization in rat BM-MSCs and DPSCs cultures, but not in ASCs. In another study, mineralization was not promoted with the addition of dEMCs on cultures of human BM-MSCs and ASCs, contrary to the DPSCs¹³. Arguably, these findings suggest that there may be a different effect of dEMCs on stromal cell mineralization depending on the origin of the stromal cells. To date, no research has been conducted yet with regard to the effect on dEMCs on human UC-MSCs.

The primary aim of this study was to investigate the effect of human dEMCs on the cell viability, proliferation capacity and mineralization potential of various human post-natal MSCs, including UC-MSCs. Furthermore, a comparative assessment of the micro-architecture of the mineralized stromal cell cultures was pursued.

Materials and Methods

Human stromal cell isolation and culture

For the DPSCs and ASCs, all samples were collected after patients' informed consent, considered waste material and their use was approved for research purposes by the Institutional Review Board of the University Medical Center Groningen, the Netherlands (registration number 201501165). The study was judged as not falling under the scope of the Medical-Scientific Act for research with humans (METc 2015.584). Dental pulp was retrieved from immature impacted third molars that were extracted from young patients (16-18 years old) who presented for scheduled tooth extraction at the Oral and

Maxillofacial Surgery Department, University Medical Center Groningen, the Netherlands. Human subcutaneous adipose tissue samples from healthy human subjects with (Body Mass Index < 30) were obtained after liposuction surgery (Bergman Clinics, the Netherlands). UC-MSCs were kindly provided by the Future Health Biobank (Nottingham, UK).

Isolation of human DPSCs and ASCs was performed as described previously^{21,22}. The cells were cultured in DMEM (Lonza Biowhittaker, Verviers, Belgium) supplemented with 10% fetal bovine serum (FBS) (Thermo Scientific, Hemel Hempstead, UK), 2 mM L-glutamine (Lonza Biowhittaker, Verviers, Belgium) and 100 U/ml Penicillin/Streptomycin (Gibco, Invitrogen, Carlsbad, CA) and incubated in a humidified incubator at 37 °C with 5% CO₂ (passage 0). Cells were expanded and passages 3-5 were used for all experiments.

For the isolation of human UC-MSCs, a transverse slice of umbilical cord tissue, taken from a region as close as possible to the placenta, was incubated in culture medium (CellGro, CellGenix, Germany) supplemented with collagenase solution (Nordmark, Germany) and antibiotic-antimycotic (Gibco, UK) under constant shaking, at 37 °C, overnight. Next day, the digest was passed through a 100 µM cell strainer and rinsed with pre-warmed CellGro, supplemented with FBS (Gibco, UK) and antibiotic-antimycotic (complete growth medium). The cell suspension was transferred to a 25-cm² cell culture flask and incubated in a humidified incubator at 37 °C with 5% CO₂. Medium replacement was performed every 3-4 days, until cells reached nearly confluency. Following sub-culturing, 2nd passage cells were counted using a haemocytometer, pelleted by centrifugation and re-suspended in cryoprotectant (10% DMSO/1% Dextran with complete medium). Finally, cell suspension was transferred to cryovials, frozen to -150 °C in a controlled rate freezer and transferred to nitrogen vapor phase storage. Cells were expanded and passages 3-5 were used for all experiments.

Cluster of differentiation (CD) expression analysis and multilineage differentiation potential

For human DPSCs and ASCs, CD surface marker expression analysis and multilineage differentiation potential were performed at 3rd passage cells according to protocols previously described²³.

For the CD surface marker expression of human UC-MSCs, 3rd passage cells were suspended in 0.9% saline and divided in four tubes. In the first tube, no anti-human fluorochrome-conjugated antibodies were added. During the analysis, the rest of the three tubes always contained the same double set of negative CD surface markers and a double set of positive markers. The tubes were placed in the dark to incubate for a period of 20 min. The anti-human monoclonal antibodies used as negative surface markers used were: CD34-ECD conjugated antibody IgG1 and CD45-PC5 conjugated antibody IgG1. The respective positive surface markers were: CD29-FITC conjugated antibody IgG2a, CD44-PE conjugated antibody IgG1, CD90-FITC conjugated antibody IgG1, CD105-PE conjugated antibody IgG3 and CD73-PE conjugated antibody IgG1K. All fluorochromes were supplied by Beckman Coulter Ltd and the analysis was performed with the FC500 flow cytometer (Beckman Coulter Ltd.).

For the multilineage differentiation potential of UC-MSCs, 3rd passage cells were plated at a cell density of 1×10^4 cells/cm² in complete growth medium in 12-well culture plates (Costar®, Corning Inc.). When cell reached nearly confluency, the culture medium was replaced with osteogenic or adipogenic basal medium (StemPro®, Gibco) supplemented with 10% osteogenic or adipogenic supplements respectively (StemPro®, Gibco) and 1% antibiotic/antimycotic, according to the manufacturer's recommendations. The media were replaced every 2-3 days and Alizarin Red-S and Oil-Red-O staining was carried out after 21 days to determine cell osteogenic and adipogenic differentiation, respectively. To confirm their chondrogenic differentiation, a modified high-density cell micropellet culture protocol was followed²⁴. Briefly, 5×10^5 cells/15ml-polypropylene tube (Sarstedt Ltd, Leicester, UK) were centrifuged at 400 Xg for 5 min, followed by a second centrifugation step at 200 xg for 5 min in 0.5 ml of either chondrogenic differentiating medium [chondrogenic basal medium (StemPro®, Gibco) completed with 10% chondrogenic

supplements (StemPro[®], Gibco) and 1% antibiotic/antimycotic or chondrogenic control medium [chondrogenic basal medium (StemPro[®], Gibco)] and 1% antibiotic/antimycotic. The pellets obtained were incubated at 37 °C and 5% CO₂ and left undisturbed for 48 h. Subsequently, the media were carefully replaced every 3 days for a total of 3 weeks. Finally, the pellets were harvested, fixed and processed using a method previously described²⁵. Paraffin-embedded sections were cleared and hydrated and then stained with 1% Alcian Blue dye solution (Sigma, St Louis, MO, USA) to detect the glycosaminoglycan components of the cartilage within the pellets, indicative of functional chondrocytes. The nuclei were counter-stained with 0.1% Nuclear Fast Red solution (Sigma, St Louis, MO, USA). Bright-field images were taken at random in each well using an inverted light microscope (Leica DMI1, Leica Microsystems) coupled with a 5-megapixel digital camera (Leica MC170-HD, Leica Microsystems). All the images were acquired and processed with the Leica Application Suite (LAS V4.9, Leica Microsystems) software.

Extraction of dEMCs

Non-carious human teeth were collected from patients presented for tooth extraction at the Oral and Maxillofacial Surgery Department, University Medical Center Groningen. All samples were collected after patients' informed consent, considered waste material and their use approved for research purposes by the Institutional Review Board of the University Medical Center Groningen, the Netherlands. dEMCs were isolated from powdered human dentin based on the EDTA-demineralization protocol previously established²⁰.

Cell viability

Cells were seeded onto flat bottom multi-well plates (Corning[®] Costar[®] 96-Well Cell Culture Plates, Sigma-Aldrich) at cell densities of 2×10^3 cells/well (72 h assay) or 1×10^3 cells/well (144h assay) and incubated with 150 μ l culture medium supplemented with dEMCs (5, 1 and 0.1 mg/ml) in a humidified incubator at 37 °C with 5% CO₂. Cells cultured in plain culture medium served as controls. For the 144h assay, the media were refreshed once at 72 h. At the end-points of each assay, a MTT assay (3-(4,5-dimethylthiazol-2-yl)-2,5-diphenyltetrazolium bromide) (Sigma-Aldrich, Amsterdam, the Netherlands) was

performed. Briefly, 0.5 mg/ml MTT was added to the wells and the plates were incubated for 4 h in a humidified incubator at 37 °C with 5% CO₂. Subsequently, the media were decanted and 150 µl of DMSO (Dimethyl Sulfoxide) (Sigma-Aldrich, Amsterdam, the Netherlands) was added to each well. Absorbance was measured at a wavelength of 570 nm (with a reference filter of 650 nm) with a Benchmark microplate reader (Bio-Rad Laboratories, Hercules, CA). The assay was repeated 3 independent times (cell cultures) with triplicate samples for each group.

Proliferation capacity

Cells were cultured as described previously for the cell viability assay at cell densities of 2×10^3 cells/well. After 72 h, immunocytochemical staining of the human Ki-67 proliferation marker was performed. Briefly, following 30 min fixation in 2% PFA in PBS, the cells were washed with PBS and permeabilized with 0.5% Triton X-100 (Sigma-Aldrich, MO, USA) in PBS for 10 min. Next, they were incubated with 10% goat serum in PBS for 30 min to prevent non-specific binding of primary antibodies. This was followed by incubation at room temperature for 90 min with anti-human Ki-67 rabbit monoclonal antibody (Abcam, the Netherlands), diluted 1:250 in PBS containing 10% donkey serum and 1 µg/ml 4',6-diamidino-2-phenylindole (DAPI). Subsequently, samples were washed with 0.05% Tween-20 in PBS and incubated in dark conditions at room temperature for 30 min with donkey anti-rabbit IgG (H+L) cross-adsorbed Alexa Fluor 594-conjugated secondary antibody (Invitrogen), diluted 1:500 in 2% normal human serum in PBS. Finally, after thorough washing steps with 0.05% Tween-20 in PBS, the TissueFAXS microscopy system (TissueGnostics GmbH, Vienna, Austria) was used to fully scan each well with the DAPI and Texas Red filters at 10x magnification sequentially. Analysis of the captured images was carried out with Tissue Quest 4.01.0127 software (TissueGnostics GmbH, Vienna, Austria). Results were expressed as % of Ki-67 positively stained cells (presence of nuclear red staining) to the total of DAPI stained cells (blue nuclear staining). The assay was repeated 3 independent times (cell cultures) with triplicate samples for each group.

In vitro mineralization assay

Cells were seeded onto clear flat bottom black multi-well plates at a cell density of 5×10^3 cells/well and incubated with 150 μ l culture medium in a humidified incubator at 37 °C with 5% CO₂ for 24 h. Next day, 150 μ l of either plain culture media or osteogenic media was added to each well, all supplemented with dEMCs (1 and 0.1 mg/ml). Cells cultured in above media, but without the addition of dEMCs served as negative and positive mineralization controls. Media were refreshed every 3 days and cells were cultured for 21 days.

Mineralization was assessed with the fluorogenic OsteoImage Mineralization Assay kit (Lonza, Walkersville, MD), which specifically binds to the hydroxyapatite portion of the mineralized depositions. The staining was performed according to the manufacturer's instructions. Additionally, 1 μ g/ml DAPI was also added to the OsteoImage staining reagent as a counter-stain of the cells' nuclei. Overlay pictures (DAPI and GFP channels) were captured with the EVOS FL Cell Imaging System (ThermoFisher Scientific) and quantification of the fluorogenic staining was performed using a FLUOstar Omega Plate Reader (BMG LABTECH, ThermoFisher Scientific) (excitation 492 nm/ emission 520 nm for OsteoImage and excitation 358 nm/ emission 461 nm for DAPI). The relative fluorescence intensity units (RFI) of the green fluorescent staining (proportional to the amount of hydroxyapatite) were normalized to the RFI of the blue DAPI staining (cell-normalized hydroxyapatite formation). The assay was repeated 3 independent times (cell cultures) with triplicate samples for each group.

Additionally, Alizarin Red-S (AR-S) staining was performed after the 21-day osteogenic induction of the cells as an extra screening validation of the extracellular mineral deposition. Images were captured with an inverted light microscope (Leica Microsystems DM IL).

Microstructural analysis of mineralized deposits (Scanning Electron Microscopy-SEM and Energy Dispersive X-ray Spectrometry-SEM-EDX)

Cells were seeded onto Thermanox coverslips (Nalge Nunc Int., Rochester, NY) in 24-well plates at a cell density of 2×10^4 cells/coverslip and incubated with culture medium. Upon reaching confluency, culture and osteogenic medium, without and with dEMCs (1 and 0.1 mg/ml) was added and samples were cultured for 21 days. Samples were fixed in 2% glutaraldehyde/2% PFA in 0.1 M sodium cacodylate buffer (Na-caco) for 60 min, followed by one time washing with Na-caco. Subsequently, they were post-fixed in 1% osmium tetroxide (OsO_4) in 0.1 M Na-caco at room temperature for 60 min and washed three more times with ultrapure water. Next, samples were dehydrated in 15 min baths with a graded ethanol series (30, 50 and 70%), followed by three 30-min baths with 100% ethanol and critical point-dried using CO_2 in a Bal-Tec 030 CPD (Balzers, Liechtenstein). Coverslips were attached to stubs using conductive double-side carbon adhesive tapes and cultures were finally sputter-coated with 5nm palladium-gold (Leica EM SCD 050). Imaging was performed in a Zeiss Supra55 SEM. Secondary electron detection was done using the Everhart-Thornley detector at 3 kV, 30 μm aperture, at 4.1 mm working distance. All images were recorded at 3072 x 2304 pixels. Contrast and brightness were adjusted based on a live histogram. SEM-EDX detection was performed with X-Max 150 detector (Oxford Instruments) at 15 kV, 60 μm aperture, beam current 4.5 nA and at 4.1 mm working distance. Acquisition was performed at 1024 pixels, with 2048 eV channels, a pixel dwell time of 50 μs and a total of 20 frames acquisition.

Statistical analysis

Statistical analysis was performed using SPSS 22.00 package (SPSS Inc., USA). All data are expressed as mean \pm standard deviation (SD). Normality of data distribution was assessed with the Shapiro-Wilk test. One-way analysis of variance (ANOVA) with a Tukey's HSD post-hoc test was performed to assess the effect of dEMCs on the cell viability and proliferation within each MSCs type. Two-way ANOVA was performed to assess the effect of dEMCs and MSCs type (independent variables) on the cell-normalized hydroxyapatite formation

(outcome measure), as measured with the fluorogenic-based OsteoImage assay. Differences were considered to be statistically significant at p-values ≤ 0.05 .

Results

Multilineage differentiation capacity and immunophenotypical analysis of cell surface markers of human MSCs (Supplemental Figures S1-2)

The osteogenic and adipogenic differentiation of DPSCs, UCMSCs and ASCs was verified by AR-S and Oil-Red-O staining respectively; smooth muscle differentiation of DPSCs and ASCs was verified by phalloidin-FITC staining; chondrogenic differentiation of UC-MSCs was verified by Alcian blue staining of paraffin-embedded sections of cell micropellets (Fig. S1). Furthermore, immunophenotypical analysis of CD surface markers for DPSCs and ASCs, revealed high positivity for those associated with mesenchymal stromal cell phenotypes (CD- 29, 44, 90 and 105) and extremely low positivity for those associated with endothelial (CD31) and hematopoietic (CD45) cells; for UC-MSCs, the mesenchymal stromal cell surface markers CD- 29, 44, 73, 90 and 105 were highly expressed, whereas the hematopoietic markers CD34 and CD45 were barely detected (Fig. S2).

dEMCs evoke a dose-dependent reduction in viable cell number

DPSCs and UC-MSCs showed a significant dose-dependent reduction of cell viability upon exposure to increasing concentrations of dEMCs, both at 72 h (Fig. 1A) and 144 h (Fig. 1B). In the higher dEMCs concentrations (5 mg/ml and 1 mg/ml), number of viable cells remained depressed throughout the exposure period, with the 5 mg/ml resulting in almost complete loss of viable cells after 144 h (Fig. 1B). Cells exposed to the lower concentration (0.1 mg/ml) showed a gradual low increase in cell viable numbers over time.

ASCs exhibited a less abrupt viable cell number decrease compared to the DPSCs and UC-MSCs. ASCs exposed to 1 mg/ml dEMCs for 72 h showed increased viability compared to the ASCs exposed to the other dEMCs concentrations (Fig. 1B). After 144 h, increased viable cell number in ASCs cultures treated with 0.1 mg/ml dEMCs was recorded compared to the higher dEMCs concentrations (Fig. 1B). Again, the 5 mg/ml resulted in almost complete loss of viable cells after 144 h (Fig. 1B).

dEMCs reduce the proliferation of the DPSCs and UC-MSCs, but not ASCs, in a dose-dependent fashion

The effect of dEMCs on cell proliferation was further investigated using the proliferation marker Ki-67 (Fig. 2A). An inverse relationship between concentration and proliferation was observed for DPSCs and UC-MSCs. No significant effect on ASCs was noted. More specifically, increased concentrations of dEMCs resulted in decreased cell proliferation in the DPSCs and UC-MSCs, whereas exposure of ASCs to the different concentrations yielded insignificant differences, with an overall high level of proliferation observed (Fig. 2B).

dEMCs elicit different mineralization responses from osteogenic cultures of the stromal cell types

The addition of dEMCs to non-osteogenic (plain) culture media did not induce any osteogenic differentiation.

Control MSCs osteogenic cultures were stained positive for the OsteoImage green staining (insets, Fig. 3ai-ci) and the AR-S red staining (insets, Fig. 3aii-cii), hence indicating hydroxyapatite formation and extracellular calcium deposition, respectively. However, the addition of 1 mg/ml dEMCs to osteogenic media abrogated mineralization in the MSCs cultures (Fig. 3). Even after 21 days of culture in osteogenic media, no positive OsteoImage green staining could be detected in 1mg/ml dEMCs-supplemented osteogenic cultures (Fig. 3Ai-Ci, only the blue DAPI nuclei counterstaining is visible), thereby indicating the complete lack of hydroxyapatite formation. In addition, no positive AR-S red staining could be detected in the 1mg/ml dEMCs-supplemented osteogenic cultures, thereby indicating the complete lack of extracellular calcium deposits (Fig. 3Aii-Cii).

In the absence of dEMCs, control osteogenic UC-MSCs cultures (Fig. 4Ci) exhibited the highest level of positive OsteoImage staining, hence hydroxyapatite formation, followed by DPSCs (Fig. 4Bi) and ASCs (Fig. 4Di). Also, the control DPSCs and UC-MSCs osteogenic cultures demonstrated significantly less hydroxyapatite formation, compared to the respective 0.1 mg/ml dEMCs-supplemented osteogenic cultures, while no difference was detected in the ASCs (Fig. 4A). Microscopically, the AR-S staining revealed control UC-MSCs osteogenic cultures with highly intense red-stained areas depicting extracellular calcium

depositions, followed by DPSCs and ASCs. Morphologically, osteogenic UC-MSCs cultures exhibited numerous calcium deposits of high degree of coalescence (highly intense red-stained nodules) fused within an extensive network of less intense red-stained calcium depositions (Fig. 4Cii), osteogenic DPSCs cultures exhibited an extensive network of red-stained calcium depositions of similar intensity (Fig. 4Bii) and osteogenic ASCs cultures exhibited big calcium deposits of high degree of coalescence (highly intense red-stained nodules) dispersed within a non-stained cellular substrate (Fig. 4Dii).

Osteogenic media containing 0.1 mg/ml dEMCs enhanced hydroxyapatite formation compared to osteogenic controls, both in the DPSCs and the UC-MSCs, as measured by the OsteoImage assay (Fig. 4A). In the DPSCs, OsteoImage revealed a nodular staining pattern of mineralization (Fig. 4Biii). AR-S staining demonstrated an extensive stained mineralized substrate with discrete areas of strongly stained nodular structures (Fig. 4Biv). In the UC-MSCs, mineral deposition revealed a different pattern compared to the DPSCs. OsteoImage staining disclosed areas with sparser cell density covered with coalescent nodular accretions and some distinct long stained (green) bundles interspersed (Fig. 4Ciii). The mineral conglomerates were also visible with the AR-S staining (Fig. 4Civ). The presence of dEMCs did not augment the mineral deposition in the ASCs cultures, but rather inhibited it. The reduction in mineral formation was apparent from both OsteoImage and AR-S staining (Fig. 4Diii-iv).

The tissue origin of stromal cells dictates the mineralization pattern

SEM revealed differences in the micro-architecture of the mineralized cultures. DPSCs osteogenic cultures showed a collagen-like fibril network with randomly orientated fibrils, upon which nodular mineral accretions were deposited (Fig. 5A). In the dEMCs-supplemented DPSCs osteogenic cultures, the collagen mesh appeared denser onto which coalesced mineralizing nodules were deposited (Fig. 5B). Osteogenic ASCs cultures revealed a similar fibril-like mineralization pattern, but in a substantially lower degree compared to the respective DPSCs (Fig. 5E). Addition of dEMCs did not augment the accretion of minerals, but rather suppressed it (Fig. 5F).

Osteogenic UC-MSCs cultures revealed a different structural morphology compared to the other stromal cell populations, with globular structures of different size and degree of coalescence aggregated upon a poorly organized fibril-like network (Fig. 5C, D). Some fibril network was present in the control UC-MSCs osteogenic cultures (Fig. 5C), while a very sparse fibril mesh-like arrangement was observed in the dEMCs-supplemented osteogenic cultures, mostly inter-connecting some coalesced aggregates (Fig. 5D). Nodular accretions seemed mainly to bud directly from the cellular bodies without any intercalating fibrils both in the control and the dEMCs-supplemented osteogenic UC-MSCs cultures. Regions with isolated individual accretions and regions with highly amassed deposits were also noted.

The elemental analysis of dEMCs-supplemented osteogenic cultures of DPSCs (Fig. 6A) and UC-MSCs (Fig. 6B) revealed the presence of the basic elements of hydroxyapatite, namely calcium (Ca) and phosphorus (P). In addition, the X-ray maps disclosed the dense accretion of hydroxyapatite-like structures of varying sizes, comprised primarily of Ca, P and O.

Discussion

The main finding of this study was that dEMCs augmented differentiation and mineralization of human MSCs osteogenic cultures in a heterogeneous fashion depending on the stromal cell origin. UC-MSCs exhibited the highest formation of hydroxyapatite-like structures, followed by the DPSCs. This was associated with reduction in their proliferation. In contrast, mineral production from ASCs was inhibited by dEMCs, coinciding with an increase in cell proliferation. A secondary finding was that the mineral deposition pattern showed stromal cell origin-dependent differences.

This is the first study to report on the mineralization potential of human UC-MSCs in combination with dEMCs. The addition of 0.1 mg/ml dEMCs in UC-MSCs osteogenic cultures resulted in a significant increase in the hydroxyapatite formation, significantly outperforming the respective yield of DPSCs and ASCs. This study did not address the mechanisms underlying these differences, but the involvement of the mitogen-activated protein kinase (MAPK) signaling pathways cannot be excluded. Indeed, the osteogenic capacity of UC-MSCs has been corroborated, with evidence pointing to the MAPK family as

the regulator of this *in vitro*-induced mineralization²⁶. In addition, the osteogenic/dentinogenic differentiation of BM-MSCs is augmented in the presence of dEMCs via increased MAPK pathway activation²⁷. Moreover, MAPK activation has been shown to mediate the enhanced mineralization of DPSCs exposed to a demineralized dentin matrix substrate²⁸. Therefore, a valid hypothesis accounting for the increased mineralization observed in the dEMCs-supplemented UC-MSCs would involve the dEMCs-induced activation of the MAPK signaling pathway. Further investigation of this hypothesis seems justified.

However, given the abundant presence of TGF- β , FGF-2 and BMP-2 in demineralized dentin matrix extracts^{15,16,29}, several molecular mechanisms become relevant. Arguably, the qualitative and quantitative composition of the dentin matrix extracts would determine the differentiation cell fate of the UC-MSCs. The FGF-2 and/ or BMP-2/MAPK/Runx2³⁰⁻³³ or the BMP-2/Dlx5/Runx2³⁴ signaling axes could underlie the increased mineralization noticed, also indicating the osteogenic differentiation of the UC-MSCs³⁵. On the other hand, TGF- β 1 could engage the Smad-dependent TGF- β 1 signaling axis³⁶, which consequentially would result in the repression of the transcriptional activity of Runx2³⁷ and favour the dentinogenic differentiation of the UC-MSCs, as has been demonstrated for the DPSCs³⁸. Especially with regard to the potential dentinogenic commitment of the UC-MSCs, the increased dEMCs-induced hydroxyapatite formation shown in the present study in the presence of dEMCs, together with their demonstrated dentinogenic differentiation under the influence of demineralized dentin matrix³⁹, could further support their use for stromal cell-mediated tooth regeneration/ tissue engineering. Remarkably though, the micro-architecture of the mineralized tissues formed by the UC-MSCs, with the large-sized globular mineral deposits laid upon a poorly organized collagenous substrate, appeared to differ from dentin, where a calcified collagen network stands. Finally, it is also possible that the complex bioactive makeup of the dEMCs could provide UC-MSCs with multiple signals, thus promoting the generation of hybrid dentin-/bone-like mineralized structures⁴⁰. Further research is warranted on the phenotype UC-MSCs acquire upon exposure to demineralized dentin matrix, as well as on the underlying mechanisms that govern the enhanced dEMCs-induced mineralization noted.

Notably, UC-MSCs had a higher intrinsic mineralization capacity than hard-tissue related DPSCs, namely, in the absence of dEMCs, UC-MSCs showed a significantly higher hydroxyapatite formation capacity than the DPSCs. The more immature state of UC-MSCs compared to DPSCs might drive their higher potency. However, the micro-architecture of the mineralized DPSCs cultures resembled more the typical structure of mineralized collagen matrix-supported tissues, such as bone and dentin. Extracted components from human dentin constitute part of the DPSCs niche. The abundant presence of TGF- β 1 in demineralized dentin matrix extracts and its stimulatory effect on the mineralization capacity of dental pulp cells have been recently demonstrated¹⁵. TGF- β 1 regulates collagen synthesis in dental pulp cells and collagen production has been positively associated with increased concentrations of TGF- β 1⁴¹. This could account for the collagen-based hydroxyapatite formation of the dEMCs-supplemented DPSCs osteogenic cultures. In contrast, high concentrations of TGF- β 1 decrease the expression of collagen and ECM-related genes in UC-MSCs or up-regulate the expression of matrix metalloproteinases⁴², which could explain the formation of dense mineralized aggregations upon a lesser organized fibril network that was observed in the respective UC-MSCs cultures in this study.

Additionally, the embryologic origin of the two stromal cell types could contribute to the differences observed in their mineralization pattern. DPSCs derive from the neural crest cells, which are involved in the formation of the majority of the collagen-based mineralized craniofacial structures⁴³. UC-MSCs may represent a more primitive stromal cell population that exhibits a different sensitivity when exposed to mineralization-inductive conditions⁴⁴. Therefore, it could be argued that DPSCs show a propensity for laying down collagen-based mineralized structures compared to UC-MSCs.

Osteogenic ASCs cultures did not benefit from the addition of dEMCs. Indeed, mineralization was impaired in the presence of dEMCs, in contrast to the other stromal cell types. The reduced mineralization capacity of dEMCs-supplemented rodent-derived ASCs cultures compared to donor-matched BM-MSCs and DPSCs has previously been demonstrated¹⁸. These results indicate that human ASCs are not responsive to components contained in the dentin matrix extract. An altered TGF β -receptor and bone

morphogenetic protein profile has been reported⁴⁵. Also, FGF-2 promotes the adipogenic profile of ASCs⁴⁶ and inhibits their osteogenic differentiation in a dose-dependent manner⁴⁷. The presence of these growth factors in the extracted dEMCs could account for the observed low level of mineralization in the ASC cultures¹³⁻¹⁶.

An inverse correlation was noticed between proliferation and mineralization in the presence of dEMCs. Notably, higher concentrations of dEMCs had a negative impact on cell viability, clearly indicating that there is a threshold above which the presence of dentin matrix proteins is detrimental. Nonetheless, the presence of lower concentration of dEMCs (0.1 mg/ml) decreased the proliferation activity in UC-MSCs and DPSCs cultures, while on the other hand enhanced their differentiation and mineralization. Induction of differentiation is inherently linked with reduction in cell proliferation. Therefore, it seems that the continuous presence of a low concentration “reservoir” of growth factors changes the proliferation and differentiation dynamics in favor of the latter. In addition, it has been shown that even lower concentrations of dEMCs are able to increase mineralization of several MSCs^{20,27,48}. This indicates that an optimal concentration that maximizes mineral formation should exist for which further research seems justified.

To summarize, addition of dEMCs to osteogenic cultures of different human MSCs selectively augmented their differentiation and in vitro hydroxyapatite formation. dEMCs-supplemented UC-MSCs and DPSCs osteogenic cultures showed significantly increased hydroxyapatite formation compared to control cultures, with UC-MSCs being benefited the most by the presence of dEMCs. This was in contrast to the ASCs, where the addition of dEMCs abrogated hydroxyapatite formation almost completely. However, the differences observed in the mineralization pattern of the mineralized stromal cell cultures necessitates further investigation. The absence of collagen-like fibrils as a matrix upon which mineralization occurs may have an impact the physico-mechanical properties of the mineralized tissues which is currently not known. The findings of this study suggest that harnessing UC-MSCs or DPSCs by cues provided by dEMCs may provide an advantageous stromal cell-based therapy for mineralized tissue repair and regeneration.

Acknowledgements

No special funding acknowledgements. Future Health Biobank (Nottingham Science & Technology Park, University Boulevard, Nottingham, NG7 2QP, United Kingdom) is especially acknowledged for the isolation, characterization and provision of the umbilical cord mesenchymal stromal cells (UC-MSCs).

Author Disclosure Statement

No competing financial interests exist.

References

1. Szpalski, C., Barbaro, M., Sagebin, F., and Warren, S.M. Bone tissue engineering: current strategies and techniques--part I: scaffolds. *Tissue Eng Part B Rev* **18**, 246, 2012.
2. Szpalski, C., Barbaro, M., Sagebin, F., and Warren, S.M. Bone tissue engineering: current strategies and techniques--part II: cell types. *Tissue Eng Part B Rev* **18**, 258, 2012.
3. Ma, J., Both, S.K., Yang, F., Cui, F.Z., Pan, J., Meijer, G.J., Jansen, J.A., and van den Beucken, J.J. Concise review: cell-based strategies in bone tissue engineering and regenerative medicine. *Stem Cells Transl Med* **3**, 98, 2017.
4. Caplan, A.I. Adult mesenchymal stem cells for tissue engineering versus regenerative medicine. *J Cell Physiol* **213**, 341, 2007.
5. Zhou, S., Greenberger, J.S., Epperly, M.W., Goff, J.P, Adler, C., Leboff, M.S., and Glowacki J. Age-related intrinsic changes in human bone-marrow-derived mesenchymal stem cells and their differentiation to osteoblasts. *Aging Cell* **7**, 335, 2008.
6. Wang, H.S., Hung, S.C., Peng, S.T., Huang, C.C., Wei, H.M., Guo, Y.J., Fu, Y.S., Lai, M.C., and Chen, C.C. Mesenchymal stem cells in the Wharton's jelly of the human umbilical cord. *Stem Cells* **22**, 1330, 2004.
7. Chen, W., Liu, J., Manuchehrabadi, N., Weir, M.D., Zhu, Z., and Xu, H.H. Umbilical cord and bone marrow mesenchymal stem cell seeding on macroporous calcium phosphate for bone regeneration in rat cranial defects. *Biomaterials* **34**, 9917, 2013.
8. Smith, A.J., Scheven, B.A., Takahashi, Y., Ferracane, J.L., Shelton, R.M., and Cooper, P.R. Dentine as a bioactive extracellular matrix. *Arch Oral Biol* **57**, 109, 2012.
9. Goldberg, M., and Smith, A.J. Cells and extracellular matrices of dentin and pulp: a biological basis for repair and tissue engineering. *Crit Rev Oral Biol Med* **15**, 13, 2004.
10. Ravindran, S., and George, A. Dentin Matrix Proteins in Bone Tissue Engineering. *Adv Exp Med Biol* **881**, 129, 2015.

11. Smith, A.J., and Leaver, A.G. Non-collagenous components of the organic matrix of rabbit incisor dentine. *Arch Oral Biol* **24**, 449, 1979.
12. Tabatabaei, F.S., Tatari, S., Samadi, R., and Moharamzadeh, K. Different methods of dentin processing for application in bone tissue engineering: A systematic review. *J Biomed Mater Res A* **104**, 2616, 2016.
13. Chun, S.Y., Lee, H.J., Choi, Y.A., Kim, K.M., Baek, S.H., Park, H.S., Kim, J.Y., Ahn, J.M., Cho, J.Y., Cho, D.W., Shin, H.I., and Park, E.K. Analysis of the soluble human tooth proteome and its ability to induce dentin/tooth regeneration. *Tissue Eng Part A* **17**, 181, 2011.
14. Tomson, P.L., Lumley, P.J., Alexander, M.Y., Smith, A.J., and Cooper, P.R. Hepatocyte growth factor is sequestered in dentine matrix and promotes regeneration-associated events in dental pulp cells. *Cytokine* **61**, 622, 2013.
15. Widbiller, M., Eidt, A., Lindner, S.R., Hiller, K.A., Schweikl, H., Buchalla, W., and Galler, K.M. Dentine matrix proteins: isolation and effects on human pulp cells. *Int Endod J* **51**(Suppl 4), e278, 2018.
16. Avery, S.J., Sadaghiani, L., Sloan, A.J., and Waddington, R.J. Analysing the bioactive makeup of demineralised dentine matrix on bone marrow mesenchymal stem cells for enhanced bone repair. *Eur Cell Mater* **34**, 1, 2017.
17. Tomson, P.L., Grover, L.M., Lumley, P.J., Sloan, A.J., Smith, A.J., Cooper, P.R. Dissolution of bio-active dentine matrix components by mineral trioxide aggregate. *J Dent* **35**, 636, 2007.
18. Tomson, P.L., Lumley, P.J., Smith, A.J., Cooper, P.R. Growth factor release from dentine matrix by pulp-capping agents promotes pulp tissue repair-associated events. *Int Endod J* **50**, 281, 2017.
19. Liu, J., Jin, T., Ritchie, H.H., Smith, A.J., and Clarkson, B.H. In vitro differentiation and mineralization of human dental pulp cells induced by dentin extract. *In Vitro Cell Dev Biol Anim* **41**, 232, 2005.

20. Davies, O.G., Cooper, P.R., Shelton, R.M., Smith, A.J., and Scheven, B.A. A comparison of the in vitro mineralisation and dentinogenic potential of mesenchymal stem cells derived from adipose tissue, bone marrow and dental pulp. *J Bone Miner Metab* **33**, 371, 2015.
21. Petridis, X., Diamanti, E., Trigas, G.Ch., Kalyvas, D., and Kitraki, E. Bone regeneration in critical-size calvarial defects using human dental pulp cells in an extracellular matrix-based scaffold. *J Craniomaxillofac Surg* **43**, 483, 2015.
22. Przybyt, E., Krenning, G., Brinker, M.G., and Harmsen, M.C. Adipose stromal cells primed with hypoxia and inflammation enhance cardiomyocyte proliferation rate in vitro through STAT3 and Erk1/2. *J Transl Med* **11**, 39, 2013.
23. van Dongen, J.A., Stevens, H.P., Parvizi, M., van der Lei, B., and Harmsen, M.C. The fractionation of adipose tissue procedure to obtain stromal vASCsular fractions for regenerative purposes. *Wound Repair Regen* **24**, 994, 2016.
24. Zhang, L., Su, P., Xu, C., Yang, J., Yu, W., and Huang, D. Chondrogenic differentiation of human mesenchymal stem cells: a comparison between micromass and pellet culture systems. *Biotechnol Lett* **32**, 1339, 2010.
25. Estes, B.T., and Guilak, F. Three-dimensional culture systems to induce chondrogenesis of adipose-derived stem cells. *Methods Mol Biol* **702**, 201, 2011.
26. Li, C-S., Zheng, Z., Su, X-X., Wang, F., Ling, M., Zou, M., and Zhou, H. Activation of the extracellular signal-regulated kinase signaling is critical for human umbilical cord mesenchymal stem cell osteogenic differentiation. *Biomed Res Int* **2016**, 3764372, 2016.
27. Yu, Y., Wang, L., Yu, J., Lei, G., Yan, M., Smith, G., Cooper, P.R., Tang, C., Zhang, G., and Smith, A.J. Dentin matrix proteins (DMPs) enhance differentiation of BMMSCs via ERK and P38 MAPK pathways. *Cell Tissue Res* **356**, 171, 2014.

28. Zhang, H., Liu, S., Zhou, Y., Tan, J., Che, H., Ning, F., Zhang, X., Xun, W., Huo, N., Tang, L., Deng, Z., and Jin, Y. Natural mineralized scaffolds promote the dentinogenic potential of dental pulp stem cells via the mitogen-activated protein kinase signaling pathway. *Tissue Eng Part A* **18**, 677, 2012.
29. Finkelman, R.D., Mohan, S., Jennings, J.C., Taylor, A.K., Jepsen, S., Baylink, D.J. Quantitation of growth factors IGF-I, SGF/IGF-II, and TGF-beta in human dentin. *J Bone Miner Res* **5**, 717, 1990.
30. Xiao, G., Jiang, D., Gopalakrishnan, R., Franceschi, R.T. Fibroblast growth factor 2 induction of the osteocalcin gene requires MAPK activity and phosphorylation of the osteoblast transcription factor, Cbfa1/Runx2. *J Biol Chem* **277**, 36181, 2002.
31. Park, O.J., Kim, H.J., Woo, K.M., Baek, J.H., Ryoo, H.M. FGF2-activated ERK mitogen-activated protein kinase enhances Runx2 acetylation and stabilization. *J Biol Chem* **285**, 3568, 2010.
32. Jun, J.H., Yoon, W.J., Seo, S.B., Woo, K.M., Kim, G.S., Ryoo, H.M., Baek, J.H. BMP2-activated Erk/MAP kinase stabilizes Runx2 by increasing p300 levels and histone acetyltransferase activity. *J Biol Chem* **285**, 36410, 2010.
33. Byun, M.R., Kim, A.R., Hwang, J.H., Kim, K.M., Hwang, E.S., Hong, J.H. FGF2 stimulates osteogenic differentiation through ERK induced TAZ expression. *Bone* **58**, 72, 2014.
34. Ryoo, H.M., Lee, M.H., Kim, Y.J. Critical molecular switches involved in BMP-2-induced osteogenic differentiation of mesenchymal cells. *Gene* **366**, 51, 2006.
35. Chen, Q., Shou, P., Zheng, C., Jiang, M., Cao, G., Yang, Q, et al. Fate decision of mesenchymal stem cells: adipocytes or osteoblasts? *Cell Death Differ* **23**,1128, 2016.
36. Massagué, J. How cells read TGF-beta signals. *Nat Rev Mol Cell Biol* **1**, 169, 2000.
37. Miyazono, K., Maeda, S., Imamura, T. Coordinate regulation of cell growth and differentiation by TGF-beta superfamily and Runx proteins. *Oncogene* **23**, 4232, 2004.

38. He, H., Yu, J., Liu, Y., Lu, S., Liu, H., Shi, J., Jin, Y. Effects of FGF2 and TGFbeta1 on the differentiation of human dental pulp stem cells in vitro. *Cell Biol Int* **32**, 827, 2008.
39. Yuanwei, Chen., Yongchun, Yu., Lin, Chen., Lanfeng, Ye., Junhui, Cui., Quan, Sun., et al. Human umbilical cord mesenchymal stem cells: a new therapeutic option for tooth regeneration. *Stem Cell Int* **2015**, 549432, 2015.
40. Arany, P.R., Huang, G.X., Gadish, O., Feliz, J., Weaver, J.C., Kim, J., et al. Multi-lineage MSC differentiation via engineered morphogen fields. *J Dent Res* **93**, 1250, 2014.
41. Melin, M., Joffre-Romeas, A., Farges, J.C., Couble, M.L., Magloire, H., and Bleicher, F. Effects of TGFbeta1 on dental pulp cells in cultured human tooth slices. *J Dent Res* **79**, 1689, 2000.
42. Li, D., Liu, Q., Qi, L., Dai, X., Liu, H., and Wang, Y. Low levels of TGF- β 1 enhance human umbilical cord-derived mesenchymal stem cell fibronectin production and extend survival time in a rat model of lipopolysaccharide-induced acute lung injury. *Mol Med Rep* **14**, 1681, 2016.
43. La Noce, M., Mele, L., Tirino, V., Paino, F., De Rosa, A., Naddeo, P., Papagerakis, P., Papaccio, G., and Desiderio, V. Neural crest stem cell population in craniomaxillofacial development and tissue repair. *Eur Cell Mater* **28**, 348, 2014.
44. Hsieh, J.Y., Fu, Y.S., Chang, S.J., Tsuang, Y.H., and Wang, H.W. Functional module analysis reveals differential osteogenic and stemness potentials in human mesenchymal stem cells from bone marrow and Wharton's jelly of umbilical cord. *Stem Cells Dev* **19**, 1895, 2010.
45. Hennig, T., Lorenz, H., Thiel, A., Goetzke, K., Dickhut, A., Geiger, F., and Richter, W. Reduced chondrogenic potential of adipose tissue derived stromal cells correlates with an altered TGFbeta receptor and BMP profile and is overcome by BMP-6. *J Cell Physiol* **211**, 682, 2007.

46. Kakudo, N., Shimotsuma, A., and Kusumoto, K. Fibroblast growth factor-2 stimulates adipogenic differentiation of human adipose-derived stem cells. *Biochem Biophys Res Commun* **359**, 239, 2007.

47. Quarto, N., and Longaker, M.T. FGF-2 inhibits osteogenesis in mouse adipose tissue-derived stromal cells and sustains their proliferative and osteogenic potential state. *Tissue Eng* **12**, 1405, 2006.

48. Lee, C.P., Colombo, J.S., Ayre, W.N., Sloan, A.J., and Waddington, R.J. Elucidating the cellular actions of demineralised dentine matrix extract on a clonal dental pulp stem cell population in orchestrating dental tissue repair. *J Tissue Eng* **6**, 2041731415586318 2015.

Corresponding Author: Xenos Petridis, University of Groningen, University Medical Center Groningen, Center for Dentistry and Oral Hygiene, Groningen, The Netherlands.

Telephone: +31 629464748. E-mail: x.petridis@umcg.nl

Figure legends

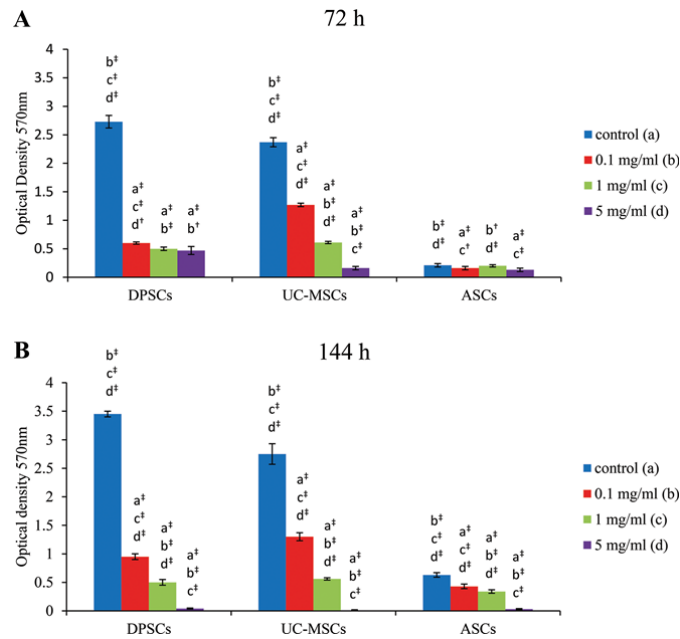


Figure 1. Dose-dependent effect of dEMCs on MSCs viability. Comparison of cell viability of human dEMCs-supplemented MSCs cultures, as assessed by MTT assay, (A) after 72 h (*one-way ANOVA* test, DPSCs: [F(3,32)=2642.758, $p < 0.001$]; UC-MSCs: [F(3,32)=3802.595, $p < 0.001$]; ASCs: [F(3,32)=18.099, $p < 0.001$] and (B) after 144 h (B) (*one-way ANOVA* test, DPSCs: [F(3,32)=10812.758, $p < 0.001$]; UC-MSCs: [F(3,32)=1386.143, $p < 0.001$]; ASCs: [F(3,32)=452.166, $p < 0.001$]. Values are represented as mean \pm SD ($n = 9$ samples per group). Small letters (a-d) denote control, 0.1, 1 and 5 mg/ml dEMCs respectively. Statistical significance is indicated by [†] for $p \leq 0.01$ and [‡] for $p \leq 0.001$ (*post-hoc Tukey HSD* test).

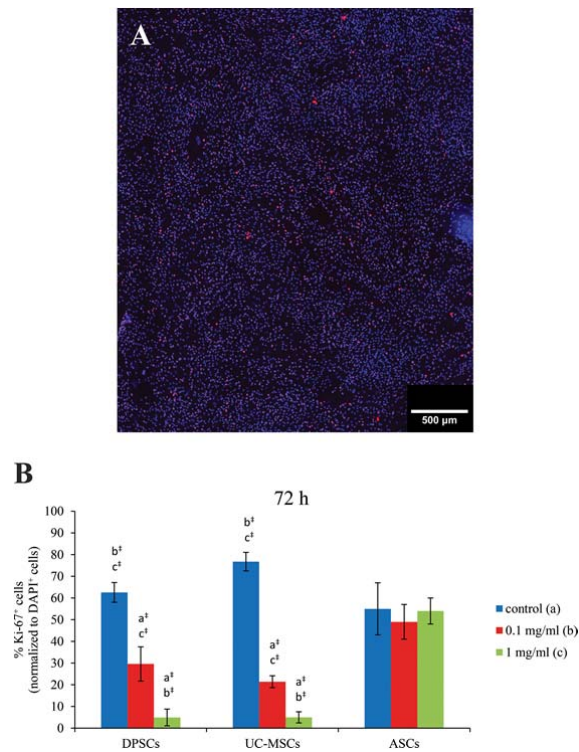


Figure 2. Dose-dependent effect of dEMCs on DPSCs and UC-MSCs proliferation, but no influence on ASCs. (A) Representative microscopic overview image (TissueFAXs microscope) from the 72 h control DPSCs culture showing the immunocytochemical staining for the proliferative marker Ki-67 (red nuclear staining) and DAPI (blue stained cell nuclei). (B) Comparison of proliferation of human dEMCs-supplemented MSCs cultures, as assessed by immunocytochemical staining of the human Ki-67 proliferation marker after 72 h (*one-way ANOVA* test, DPSCs: [F(2,24)=231.244, $p < 0.001$]; UC-MSCs: [F(2,24)=1173.219, $p < 0.001$]; ASCs: [F(2,24)=1.391, $p = 0.268$]. Values are represented as mean \pm SD (n = 9 samples per group). Small letters (a-c) denote control, 0.1 and 1mg/ml dEMCs respectively. Statistical significance is indicated by [†] for $p \leq 0.001$ (*post-hoc Tukey HSD* test).

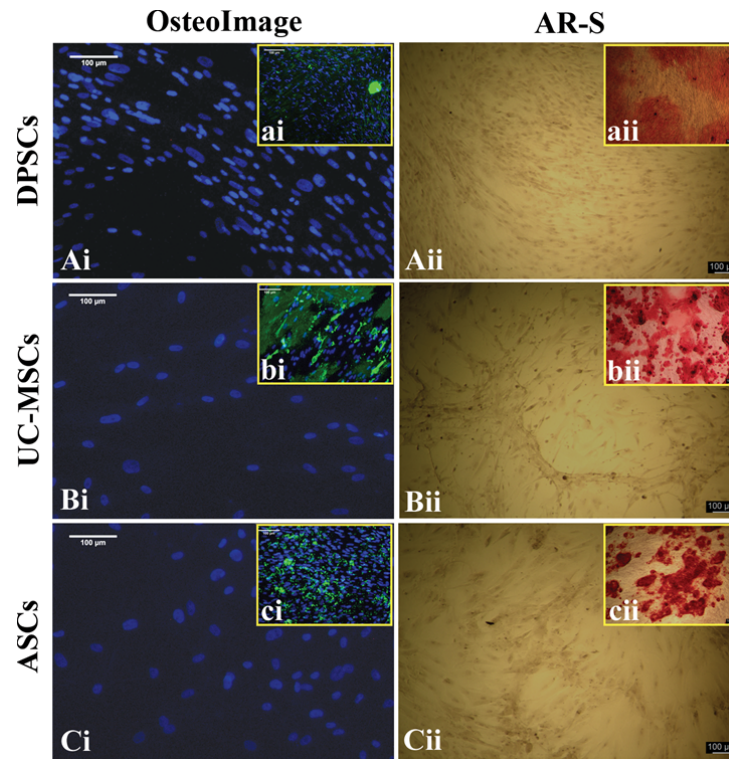


Figure 3. Abrogation of mineral deposition upon exposure of MSCs to osteogenic media supplemented with 1 mg/ml dEMCs. Representative microscopic images from control MSCs osteogenic cultures stained positive with the OsteoImage (insets, 3ai-ci, green staining) and AR-S staining (insets, 3aii-cii, red staining) and from 1 mg/ml dEMCs-supplemented MSCs osteogenic cultures stained negative with the OsteoImage (Ai-Ci) and AR-S staining (Aii-Cii).

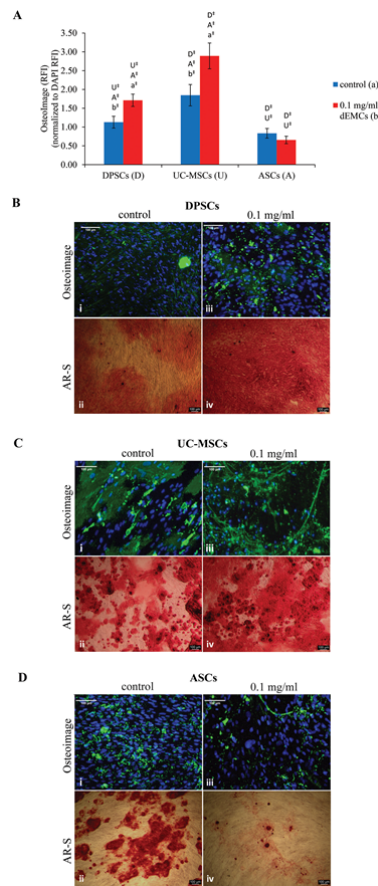


Figure 4. dEMCs enhanced the mineralization efficiency of DPSCs and UC-MSCs osteogenic cultures, but not of ASCs. (A) Comparison of the hydroxyapatite formation capacity of human MSCs osteogenic cultures in the absence and presence of 0.1 mg/ml dEMCs (A) (two-way ANOVA test, statistically significant interaction between the two independent variables, *i.e.*, dEMCs and MSCs type, [F(2,48)=37.285, p<0.001]). Values are represented as mean \pm SD (n=9 samples per group). Capital letters D, U, and A denote the MSCs used, *i.e.*, DPSCs, UC-MSCs and ASCs, respectively and small letters a and b denote the control and the 0.1 mg/ml dEMCs groups, respectively. Statistical significance is indicated by \ddagger for p \leq 0.001 (simple main effects analysis). (B-D) Representative microscopic images from control and 0.1 mg/ml dEMCs-supplemented MSCs osteogenic cultures stained with the OsteoImage fluorogenic and Alizarin Red staining. Scale bars represent 100 μ m.

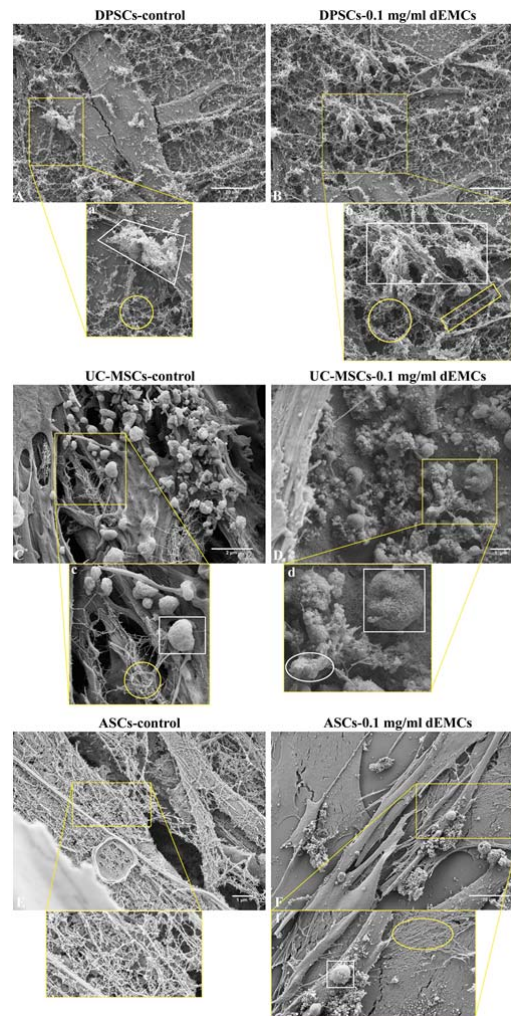


Figure 5. Scanning Electron Microscopy (SEM) imaging of the MSCs osteogenic cultures revealed distinct differences in their pattern of mineral deposition. DPSCs osteogenic cultures (A), showed a collagen network (inset a, yellow circle), upon which nodule-like minerals were deposited (inset a, white trapezoid). dEMCs-supplemented DPSCs osteogenic cultures (B), exhibited a denser collagen mesh (inset b, yellow circle), richer in mineral depositions of higher coalescence (inset b, white rectangular), while long distinct collagen fibrils were frequently noticed (inset b, yellow rectangular). UC-MSCs osteogenic cultures (C), exhibited isolated areas packed with collagen fibrils (inset c, yellow circle), but no extensive organized collagen network. Globular mineralized structures seemed to bud directly from the cellular bodies with no intercalating collagen fibrils and varied in size (inset c, white rectangular). dEMCs-supplemented UC-MSCs osteogenic cultures (D), exhibited enhanced mineral deposition, both in terms of the size of the globular mineral

deposits (inset d, white square) and the degree of coalescence of smaller mineral accretions (inset d, white ellipse). The lack of an organized collagenous substrate was a prominent feature. ASCs osteogenic cultures (E), demonstrated a collagen fibrin-associated mineralization, similar to DPSCs osteogenic cultures, but with a considerably smaller-sized amassing mineral accretions deposited on the collagen substrate (inset e). dEMCs-supplemented ASCs osteogenic cultures (F), showed a very poor collagen network (inset f, yellow circle) and only some randomly distributed mineral accretions, directly budding from the cellular bodies being observed (inset f, white square).

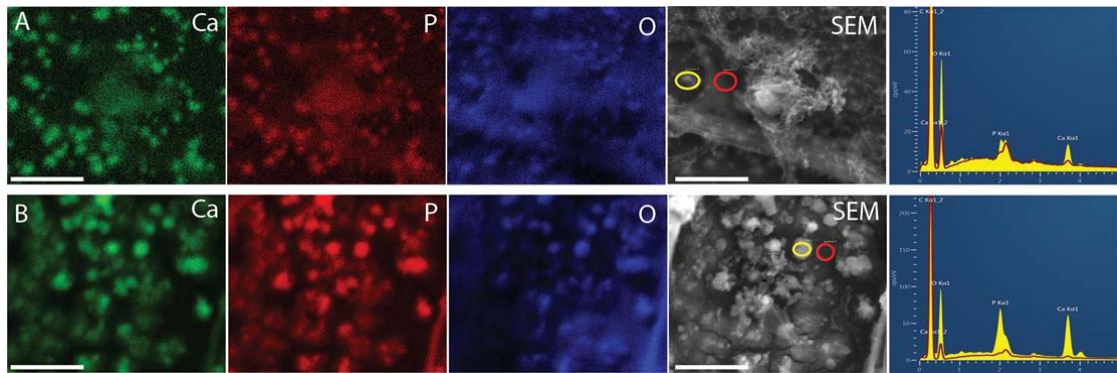
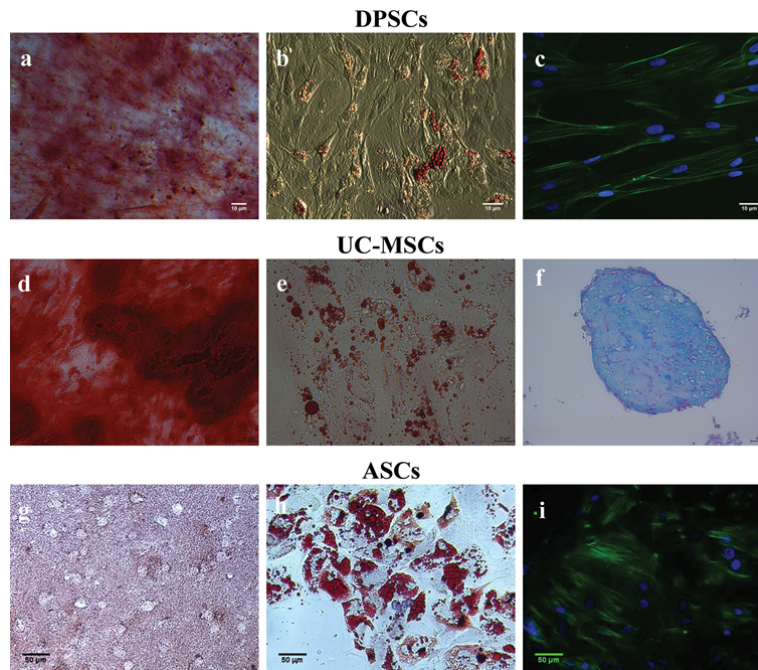
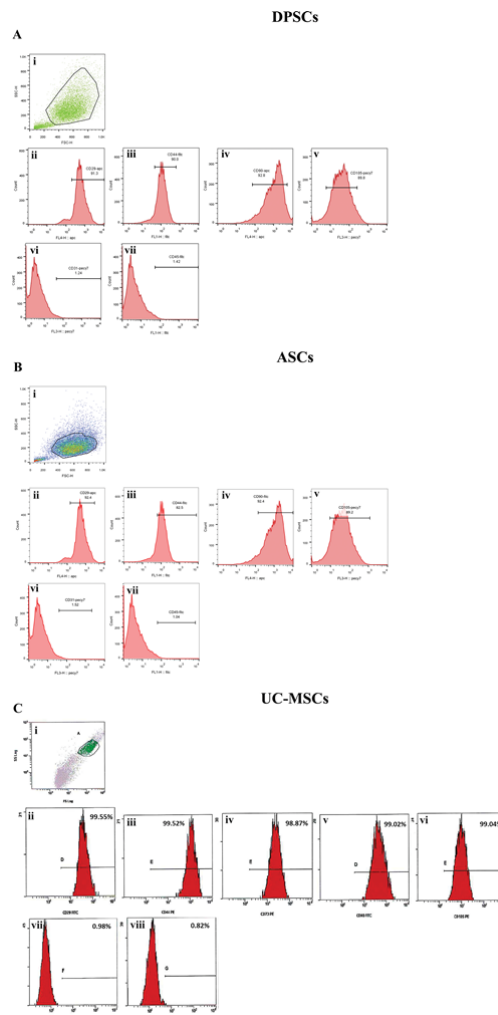


Figure 6. Scanning Electron Microscopy-based X-ray mapping verifies the hydroxyapatite-like mineral formation based on presence Ca, P, and O. Single element distribution maps generated from areas as shown by the backscattered SEM images, showing corresponding maps of calcium (green), phosphorus (red), and oxygen (blue) in dEMCs-supplemented (A) DPSCs and (B) UC-MSCs osteogenic cultures. EDX spectra show higher peaks for both calcium (Ca) and phosphorus (P) for mineralized regions (spectra in yellow from regions marked with yellow eclipses), compared to smaller Ca and P peaks for non-mineralized regions (spectra displayed as red lines from regions marked by red eclipses). Scale bars represent 5 μm .



Supplemental Figure S1. Multilineage differentiation capacity of MSCs. (a-c) Osteogenic, adipogenic and smooth muscle cell differentiation of DPSCs, as verified by AR-S staining (calcium deposits stained red), Oil-Red-O staining (lipid droplet accumulation stained red) and phalloidin-FITC and DAPI staining (F-actin stained green and nuclei stained blue), respectively. (d-f) Osteogenic, adipogenic and chondrogenic differentiation of UC-MSCs, as verified by AR-S staining (calcium deposits stained red), Oil-Red-O staining (lipid droplet accumulation stained red) and Alcian blue staining (glycosaminoglycan components of the cartilage within the micropellets stained blue), respectively. (g-i) Osteogenic, adipogenic and smooth muscle cell differentiation of ASCs, as verified by AR-S staining (calcium deposits stained red), Oil-Red-O staining (lipid droplet accumulation stained red) and phalloidin-FITC and DAPI staining (F-actin stained green and nuclei stained blue), respectively.



Supplemental Figure S2. Flow cytometry analysis of cluster of differentiation (CD) cell surface markers of MSCs. Analysis for (A) DPSCs and (B) ASCs. Dot plot (forward vs. side scatter plot) (Ai, Bi), histogram plots showing highly expressed mesenchymal stromal cell markers (CD29, CD44, CD90 and CD105) (Aii-v, Bii-v) and very low expressed markers associated with endothelial cells (CD31) (Avi, Bvi) and hematopoietic cells (CD45) (Avii, Bvii). (C) Analysis for UC-MSCs. Dot plot (forward vs. side scatter plot) (i), histogram plots showing highly expressed mesenchymal stromal cell markers (CD29, CD44, CD73, CD90 and CD105) (ii-vi) and very low expressed markers associated with hematopoietic cells (CD34 and CD45) (vii, viii).